

Differentiation of brain and retinal organoids from confluent cultures of pluripotent stem cells connected by nerve-like axonal projections of optic origin

Milan Fernando,^{1,9} Scott Lee,^{1,9} Jesse R. Wark,^{1,2} Di Xiao,^{3,5,6} Benjamin Y. Lim,¹ Michelle O'Hara-Wright,^{1,6} Hani J. Kim,^{3,5,6} Grady C. Smith,¹ Ted Wong,⁴ Erdahl T. Teber,^{4,6} Robin R. Ali,^{7,8} Pengyi Yang,^{3,5,6} Mark E. Graham,^{2,6} and Anai Gonzalez-Cordero^{1,6,*}

¹Stem Cell Medicine and Stem Cell and Organoid Facility, University of Sydney, Westmead, 2145 NSW, Australia

²Synapse Proteomics, University of Sydney, Westmead, 2145 NSW, Australia

³Computational Systems Biology, University of Sydney, Westmead, 2145 NSW, Australia

⁴Bioinformatics, Children's Medical Research Institute, University of Sydney, Westmead, 2145 NSW, Australia

⁵Charles Perkins Centre, School of Mathematics and Statistics, University of Sydney, Sydney, NSW 2006, Australia

⁶School of Medical Sciences, Faculty of Medicine and Health, University of Sydney, NSW 2006, Australia

⁷Gene and Cell Therapy Group, UCL Institute of Ophthalmology, London EC1V 9EL, UK

⁸Present address: Centre for Cell and Gene Therapy, King's College London, 8th Floor Tower Wing, Guy's Hospital, London SE1 9RT, UK

⁹These authors contributed equally

*Correspondence: agonzalez-cordero@cmri.org.au

<https://doi.org/10.1016/j.stemcr.2022.04.003>

SUMMARY

Advances in the study of neurological conditions have been possible because of pluripotent stem cell technologies and organoids. Studies have described the generation of neural ectoderm-derived retinal and brain structures from pluripotent stem cells. However, the field is still troubled by technical challenges, including high culture costs and variability. Here, we describe a simple and economical protocol that reproducibly gives rise to the neural retina and cortical brain regions from confluent cultures of stem cells. The spontaneously generated cortical organoids are transcriptionally comparable with organoids generated by other methods. Furthermore, these organoids showed spontaneous functional network activity and proteomic analysis confirmed organoids maturity. The generation of retinal and brain organoids in close proximity enabled their mutual isolation. Suspension culture of this complex organoid system demonstrated the formation of nerve-like structures connecting retinal and brain organoids, which might facilitate the investigation of neurological diseases of the eye and brain.

INTRODUCTION

The rapidly progressing field of human pluripotent stem cells (hPSCs), including embryonic stem cells (ESCs) and induced pluripotent stem cells (iPSCs) and their derivative organoids, continues to provide new insights into basic biology, human development, modeling of human diseases, and discovery of innovative treatments. Neural differentiation has been extensively studied, improving our understanding of the mechanism of neurodevelopmental conditions (Qian et al., 2019). Large numbers of neurons and astrocytes can be generated using three-dimensional (3D) suspension methods that recapitulate the physiological niche and environment of the developing human brain (Paşca et al., 2015).

In the developing CNS, the eye and the brain form as an extension of the forebrain diencephalic and telencephalic region, respectively (Sinn and Wittbrodt, 2013). Brain organoids replicate specific brain regions or whole cerebral areas, with both occasionally developing eye regions (Lancaster et al., 2013; Quadrato et al., 2017). Differentiation protocols are usually classified as either guided/direct or non-guided/undirected cultures, on the basis of the necessity for the use of growth factors or their absence in non-

guided spontaneous differentiation, which relies on endogenous self-forming ability of the cells (Qian et al., 2019). Brain organoids generated using these varied methodologies have been well characterized using transcriptome analysis. Single-cell RNA sequencing (scRNA-seq) has elucidated their cellular composition and the reproducibility of protocols (Tanaka et al., 2020). Proteome studies have been rarely performed. Measurements of neuronal activity are critical to establish organoid variability, maturation and functionality.

Diseases of the eye and the brain are now understood to be more intertwined than previously thought. Studies of common conditions, such as glaucoma and Alzheimer's disease, have demonstrated degenerative changes and disease traits in both brain and eye (Ning et al., 2008). Complex organoids have the potential to provide useful models of these disease *in vitro* with the proviso that they recapitulate retinal development, morphology and maturation. Therefore, improved formation of hPSC-derived retinal-brain connection through an optic nerve is vital for effective degenerative disease modeling.

Here we hypothesized that it is possible to reproducibly generate functional brain organoids from retinal confluent cultures of PSCs. We also asked if retinal and brain



organoids developing together in suspension culture would form a complex retina-brain organoid system that would enable the formation of an optic nerve-like structure, similar to recently described assembloid systems (Fli-gor et al., 2021).

We demonstrated a non-guided, simple, and economical differentiation protocol that generated cortical brain organoids alongside of retinal vesicles from a confluent culture of hPSCs. The spontaneous generation of retinal vesicles has been previously described (Cordero et al., 2017; Reichman et al., 2014, 2017), but the differentiation and isolation of brain structures, to our knowledge, has not been described elsewhere. The ease of precisely locating brain organoids, because of morphology and their proximity to retinal vesicles, reduced organoid variability. Brain organoids were characterized as dorsal cortical organoids, which when further cultured in 3D suspension matured into functional organoids. A systematic comparison of scRNA-seq datasets revealed a close similarity of our organoids with other dorsal patterned hPSC-derived brain organoids (Velasco et al., 2019), and proteomic analysis of organoids revealed the presence of numerous synaptic markers. Organoid electrophysiological activity was dependent on culturing in relevant basal medium (Bardy et al., 2015), with proteomics providing insights into why this physiological environment aids functional activity. Finally, the generation of retinal and cortical organoids facilitated the isolation of both structures for 3D culturing, forming a complex organoid system. Notably, 3D cultured retinal-brain organoids maintained the natural association created in the dish during their spontaneous development. This enabled the formation of immature nerve bundle-like structures between the two organoids. Although at this early age in culture it is difficult to confirm the formation of true optic nerve structures, we show that retinal ganglion cell (RGC) axonal projections cross the retinal organoid to populate brain organoid regions.

RESULTS

Generation of self-forming retinal and cortical brain organoids from confluent cultures

The retina is an extension of the CNS arising from the fore-brain region in the developing embryo (Figure 1A). The schematic in Figure 1B shows that pro-neural induction of confluent cultures of pluripotent stem cells (PSCs) spontaneously generate retinal pigment epithelium (RPE) from which retinal vesicles appear. Further analysis of other structures forming in this two-dimensional (2D)/3D environment highlighted the presence of 3D regions containing clear neuronal rosettes forming adjacent to retinal vesicles. We hypothesized that these were brain vesicles.

Following a neural induction period of 4–6 weeks in culture, neuroretinal vesicles and neural rosette structures appeared (Figure 1C). These areas were dissected and grown in suspension for maturation (Figure 1D). By 6 weeks of differentiation, $39.5\% \pm 19\%$ of all organoids observed in cultures were retinal vesicles, while $60.5\% \pm 19\%$ were neuronal organoids ($n = 10$ differentiation batches), demonstrating that a proportion of organoids are generated independently and are not in proximity to retinal organoids. Immunohistochemistry (IHC) of 6-week-old retinal organoids revealed typical neuroepithelium with RXRy cone cells and HuC/HuD-positive interneurons (Figure 1E). Brain organoids contained proliferative Ki67/NCAD regions (Figure 1F) and active CASPASE3 cells (Figure S1). Neuroepithelium regions contained SOX2/NCAD-positive neural progenitor cells (Figures 1G and 1H) and were also positive for cortical FOXG1 and NESTIN/PAX6 markers (Figures 1I, 1J, and S1). These cortical organoids were negative for ventral cortex-specific marker NKX2.1, as opposed to whole cerebral organoids (Figure S1), confirming their dorsal cortical origin.

Brain organoids were easily distinguished in the confluent cultures, enabling the isolation of a population of organoids for further maturation and therefore minimizing the variability of mature cultures. We tested this protocol in twenty-two pluripotent cell lines, with twenty-one generating both retinal and brain organoids and one generating retinal organoids only. Table S1 summarizes the reproducibility of the protocol across four of these cell lines. Furthermore, IHC analysis characterized these cortical organoids (Figure S1). Cortical plate TBR1, CTIP2 cells, and SATB2-positive cells were also present. From 8 to 12 weeks in culture, organoids increased in size significantly from $2,000 \pm 560$ to $2,600 \pm 474$ μm in diameter ($n = 20$ – 25 organoids, $N = 3$ differentiation batches; mean \pm SD; $p = 0.0002$, unpaired two-tailed t test). Astrocytes positive for S100B and GFAP were present in similar percentages to TUJ1-positive neurons ($75\% \pm 14\%$ neurons versus $57\% \pm 17\%$ glial cells; $n = 10$ images from each differentiation batch; $N = 3$ or 4 differentiation batches; mean \pm SD; $p < 0.0001$, unpaired two-tailed t test). Analysis at 15 weeks demonstrated the presence of mature inhibitory gamma aminobutyric acid (GABAergic) neurons and their CALRETININ-positive subtypes (Figures 2A–2L). Imaging of organoids by light-sheet microscopy confirmed the presence of numerous CALRETININ-positive neurons and GFAP-positive astroglial cells (Video S1).

2D/3D cortical organoids have similar cell type compositions to other brain organoids

Next, we performed scRNA-seq analysis using the 10X genomics platform to further investigate the cell type composition of cortical organoids and to establish their similarity

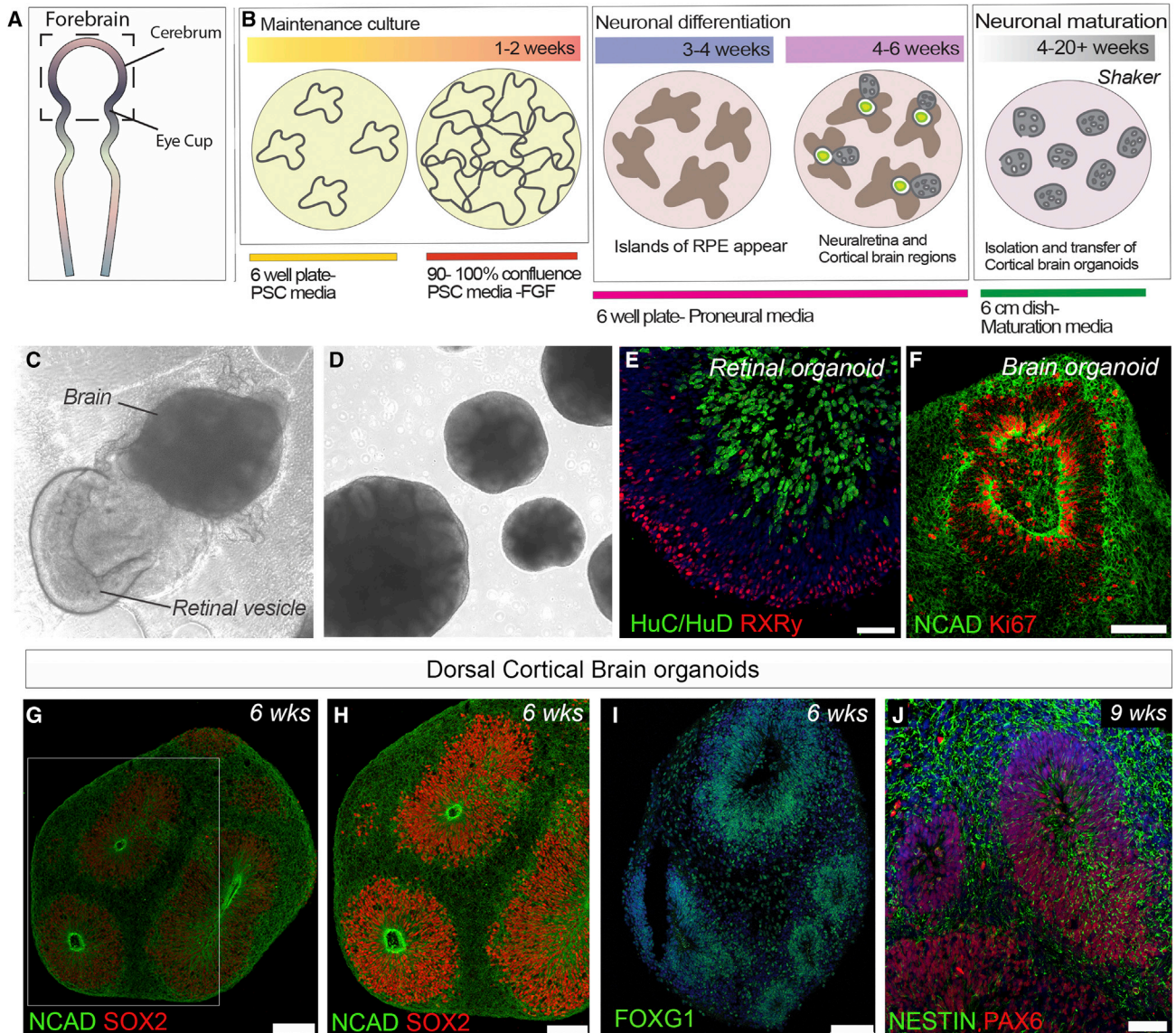


Figure 1. Confluent PSC differentiation protocol gives rise to cortical and retinal organoids

(A) Schematic illustrating neural tube formation and the formation of both cerebellum and eye cups from forebrain.
 (B) Schematic of the 2D/3D differentiation protocol timeline for both retinal and cortical organoid formation.
 (C) Image of a retinal vesicle and brain organoid in 2D culture.
 (D) Bright-field image of floating brain organoids, with typical neural rosettes, following excision from 2D culture.
 (E) Images of retinal organoid showing RXRy cone cells and HuC/HuD interneurons.
 (F) Brain organoids showing Ki67/NCAD positive neuroepithelium.
 (G–J) Cortical origin in 6-week-old brain organoids is confirmed by the presence of SOX2-, FOXG1-, and PAX6-positive neural precursor markers.

Scale bars, 50 μ m (J), 75 μ m (H), 100 μ m (E, G, and I), and 250 μ m (F). See also [Figure S1](#).

to other published brain organoid datasets, which were derived from various directed and undirected protocols. We used scClassify ([Lin et al., 2020](#)), a machine learning-based method, to annotate cell types that were present in our scRNA-seq organoids ([Figure 3A](#)). Then we compared

the composition of cell types in 3-month-old cortical organoids (COs) we generated against those from 3- and 6-month-old brain organoids and cell types from gestational week (GW) 12 pre-frontal lobe (PFL) fetal brain ([Figure 3B](#)).

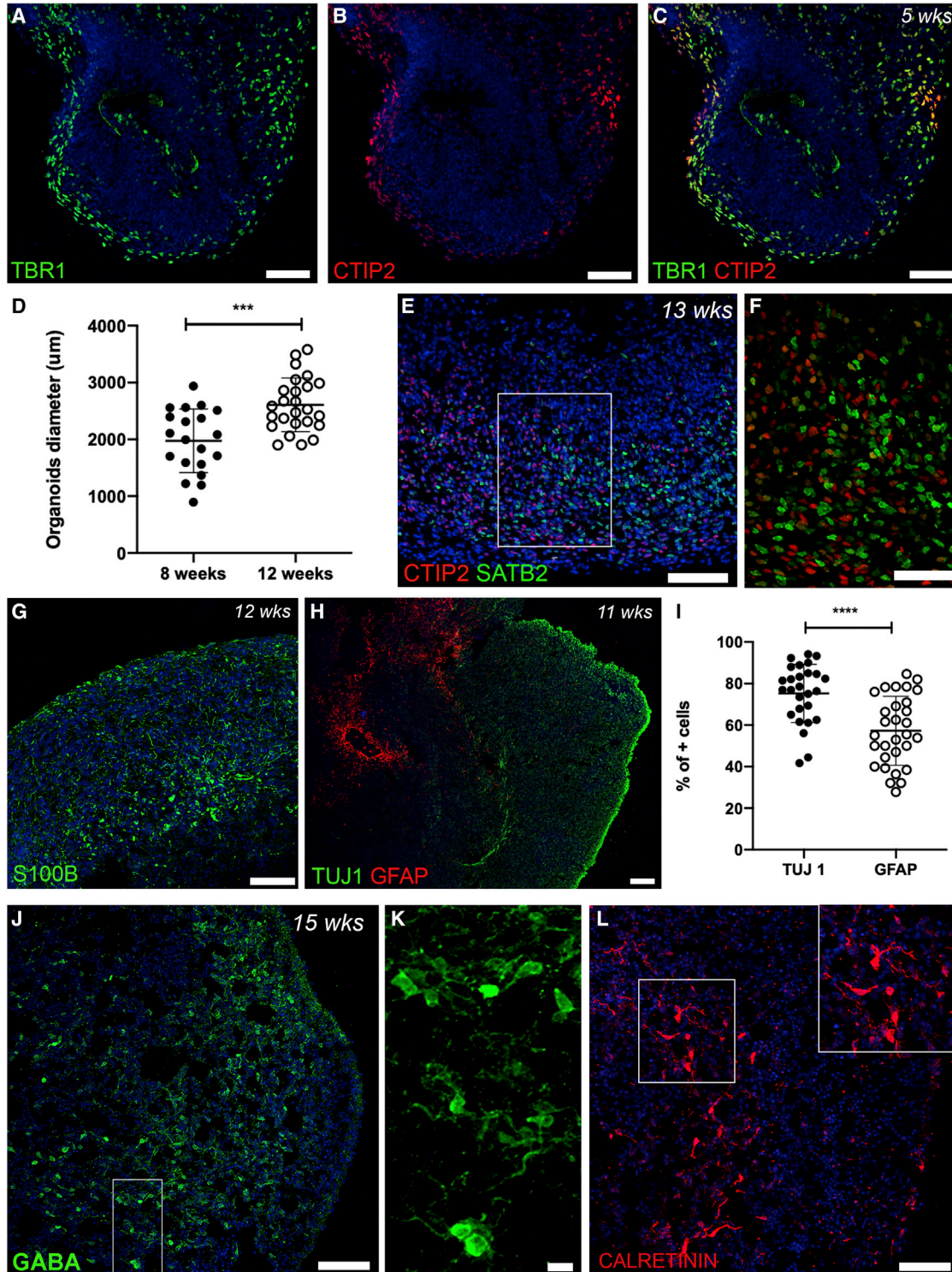


Figure 2. Cortical brain organoids generate cortical plate neurons and glial cells

(A–C) Images of week 5 cortical organoids showing the presence of TBR1 and CTIP2 cortical plate neurons.

(D) Cortical organoid diameter and significant size increase with days in culture (n = 30 organoids, N = 3 differentiation batches, mean ± SD, unpaired two-tailed t test).

(legend continued on next page)



First, we compared the composition of cell types by using the cell type labels from the original authors for each of the published datasets, summarized in [Figure 3B](#). Although the proportions of each cell type varied across protocols, the overall cell type compositions were similar. This was independent of the protocol, their method of differentiation (directed or undirected), and the age of the organoid ([Figure 3C](#)). In this analysis, Quadrato et al. data (Quad3mU) showed the most diverse cell type composition.

Next, we used scClassify to annotate cells in our CO scRNA-seq dataset by training the classification model using either each individual public dataset as a reference or using all datasets jointly (joint training) ([Figure 3D](#)). The predicted cell type composition in COs data was plotted with respect to the training data, and irrespective of the training dataset, a similar cell type composition was observed in our COs. In agreement with this, the expression profiles of key marker genes for each cell type population were also largely consistent, irrespective of the training dataset ([Figure S2](#)). BMP-responsive cells, intermediate (bright orange), and proteoglycan-expressing cell types were absent from our dataset. Note that cells are annotated as “unassigned” when they could not be classified to any cell type. Cells are annotated as “intermediate” when they could not be classified to a specific cell type but an intermediate among multiple cell types. This intermediate population (denoted with an asterisk) is different from the intermediate cell type annotated in the training datasets (bright orange). As the scClassify jointly trained using multiple reference datasets reduces both unassigned and intermediate classification, the classification result from the jointly trained model was used in the subsequent comparison. Organoid cell types were clustered in a t-distributed stochastic neighbor embedding (tSNE) plot showing that cortical neurons were the most abundant cell type ([Figure 3E](#)). We then measured the agreement between different cell type compositions across the multiple datasets using the intraclass correlation coefficient (ICC) ([Figure 3F](#)). Three major correlating groups were evident in relation to cell type compositions: (1) Velasco et al., 6 months, directed (Vela6mD); (2) Quadrato et al., 3 months, undirected (Quad3mU); and (3) the remaining protocols, which included our 2D/3D COs. In accordance with [Figure 3C](#), except for Quad3mU, all 3 month organoids and the GW12 fetal sample clustered together, suggest-

ing similar cell type composition. Notably, our organoids closely resembled the guided differentiation of dorsally patterned forebrain organoids (Vela3MD), known for their reproducibility (Velasco et al., 2019). Cell-type proportions were more diverse when Quad3mU was used as training data, suggesting a unique cell type composition in this dataset. In fact, Quad3mU cell type annotations clustered as a group with Vela6mD separate from Trujillo et al., 6 months, directed (Truj6mD) and the remaining 3 month organoids. Therefore, although cell type composition of Vela6mD appeared to be different from those of 3 month organoids, the composition of Truj6mD was more similar to 3 month organoids.

Proteome analysis of brain organoids highlights abundance of proteins related to synaptic transmission

The proteomes of iPSCs and cortical organoids were surveyed to a depth of 6,244 and 5,719 proteins, respectively (after filtering and counting only unique genes). There were 4,444 proteins shared between the iPSC (n = 3 IPS pellets from different passages) and cortical organoid lists (n = 3 organoids; N = 3 differentiation batches, 9 organoids analyzed in total). Gene Ontology enrichment analysis was performed with a focus on biological process and Kyoto Encyclopedia of Genes and Genomes (KEGG) pathway terms ([Figures 4A–4D](#)). [Figure 4A](#) shows the top thirty biological process terms that had the largest difference in significance between iPSCs and organoids. Terms related to the cell cycle, chromosomes, and DNA were more likely to be enriched for iPSCs, whereas terms related to the synapse, synaptic vesicles, vesicular transport, axon/dendrite development, and neuron projection were more enriched for cortical organoids. Next, we extracted the top five synaptic and development terms (not already shown in [Figure 4A](#)) from the list of significant biological process terms ([Table S2](#)). For example, the terms “postsynapse organization” and “regulation of postsynaptic membrane neurotransmitter receptor levels” were enriched for cortical organoids ([Figure 4B](#)). Neuron development and dendritic spine development were enriched for organoids ([Figure 4C](#)). The KEGG pathway terms ribosome biogenesis in eukaryotes, DNA replication, cell cycle, and basal transcription factors were enriched for iPSCs, while axon guidance, neurotrophin signaling pathway, and long-term

(E–H) Organoids showing CTIP2- and SATB2-positive cells (E and F; high-magnification image of inset in E shown in F) and S100B and GFAP glial cells (G and H).

(I) Percentage of cells expressing TUJ1 and GFAP per area (mm²) in 11-week-old cells (n = 10 images from 2 or 3 organoids, N = 3 differentiation batches, mean ± SD, unpaired two-tailed t test).

(J–L). Week 15 cortical organoid showing GABA- and CALRETININ-positive inhibitory neurons.

(K) shows high-magnification image of inset in (J).

Scale bars, 15 μm (K), 50 μm (F), 75 μm (A–C), and 100 μm (E, G, H, J, and L).

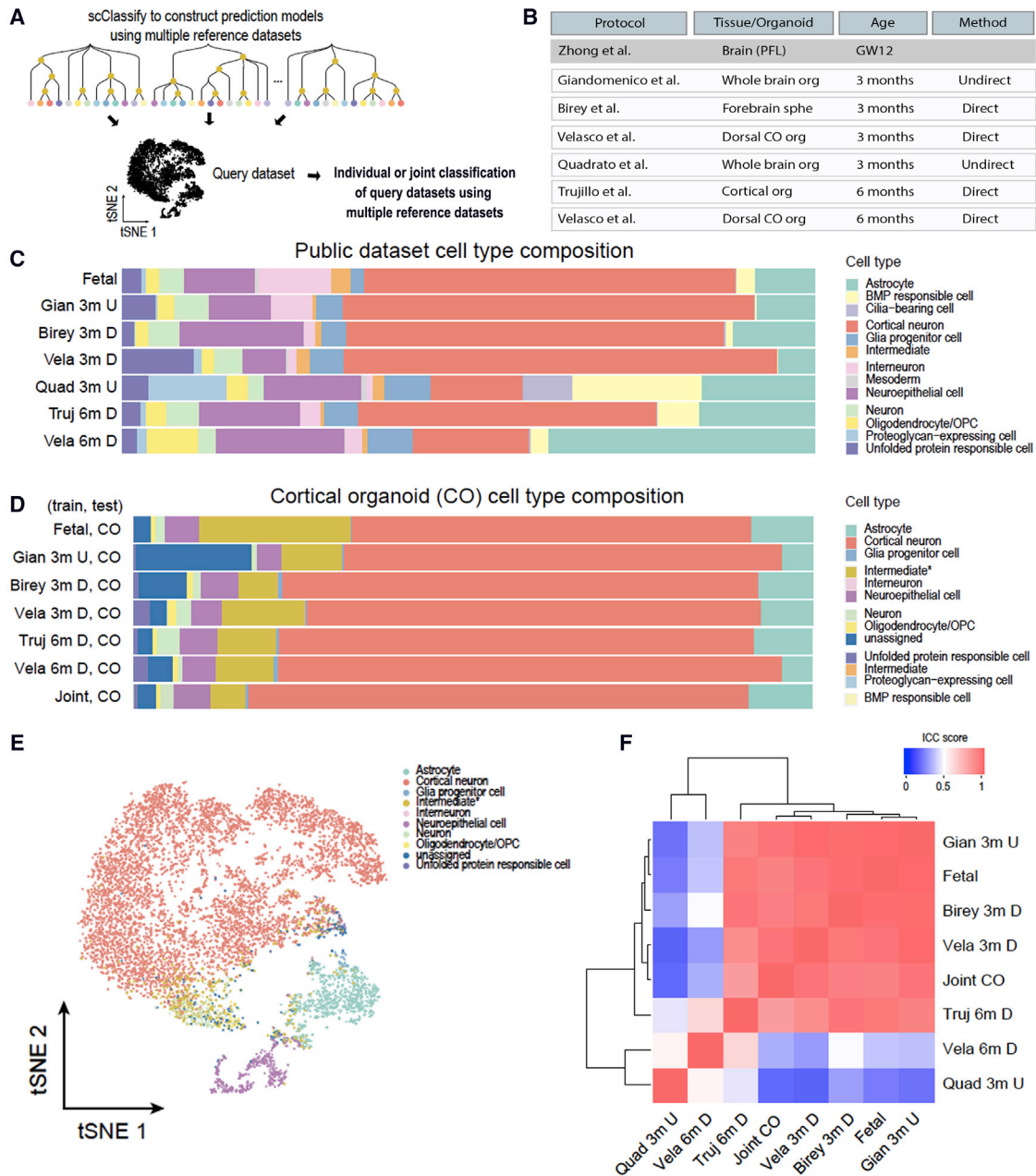
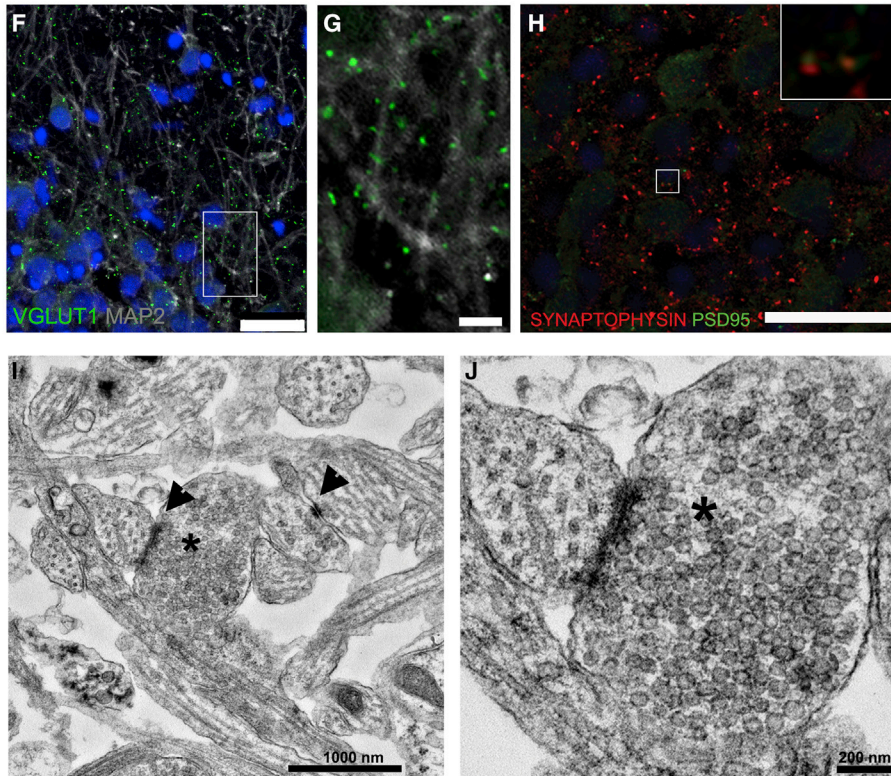
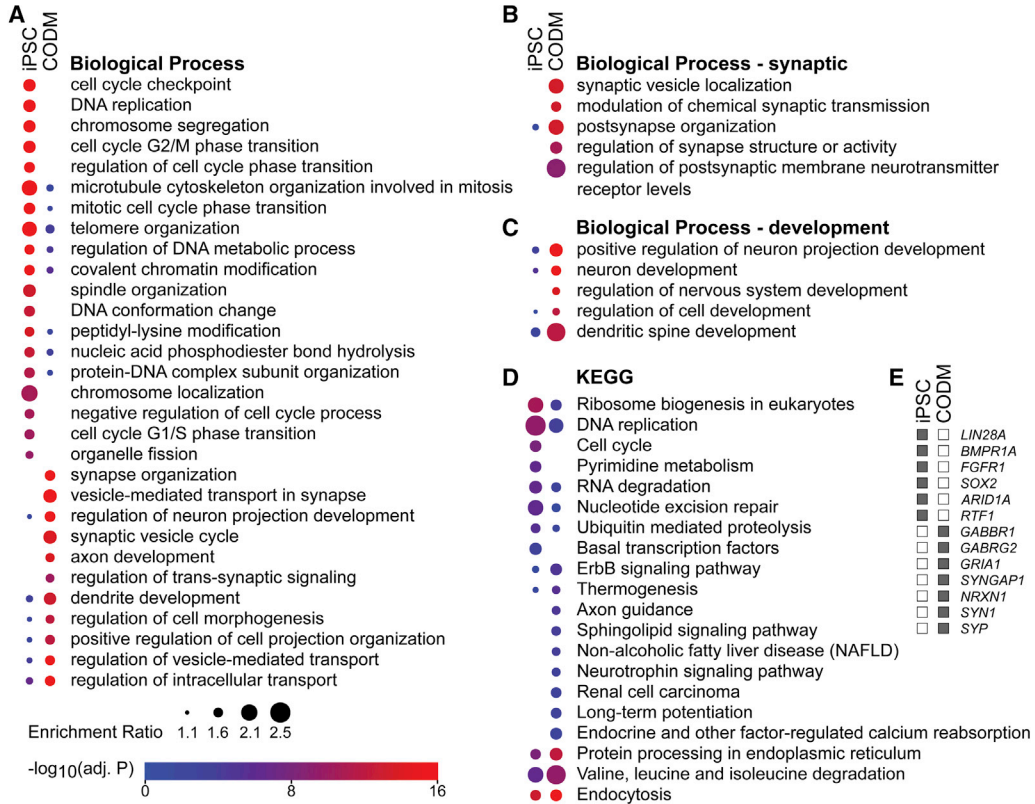


Figure 3. Comparison of cortical organoids and scRNA-seq available dataset

- (A) Schematic illustrating scClassify computational analysis to categorize a dataset using multiple reference datasets.
 (B) Table summarizing the public scRNA-seq reference datasets included in comparison and their differentiation protocols.
 (C) Cell type composition in public datasets on the basis of the annotation from their original studies.
 (D) Cell type composition in cortical organoids (COs) scRNA-seq dataset predicted by scClassify trained by each or all (i.e., joint) public datasets.
 (E) tSNE plot illustrating the cell types composition in COs on the basis of scClassify annotation using joint training.
 (F) Interclass correlation heatmap showing the agreement between cell type compositions among different organoids and a fetal brain. See also [Figure S2](#).

potentiation terms were enriched for organoids ([Figure 4D](#)). [Figure 4E](#) shows examples of detected proteins that were exclusive to the iPSCs and are involved in stem cell prolifer-

ation and maintenance. Conversely, GABA receptor subunits (encoded by *GABBR1* and *GABRG2*), a glutamate receptor subunit (encoded by *GRIA1*), a mediator of



(legend on next page)



postsynaptic plasticity (encoded by *SYNGAP1*), a transsynaptic protein (encoded by *NRXN1*) and two synaptic vesicle-associated proteins (encoded by *SYN1* and *SYP*) are examples of proteins detected exclusively in organoids (Figure 4E). The expression of these genes was also confirmed in the scRNA transcriptome dataset (Figure S2). IHC analysis confirmed synapse formation. MAP2-positive glutamatergic excitatory neurons expressing the vesicular glutamate transporter 1 (VGLUT1) protein were evident in organoids (Figures 4E and 4F [high magnification of boxed area in Figure 4E]; Figure S3). Pre-synaptic protein synaptophysin was readily detected in puncta that localized in proximity to postsynaptic density protein PSD95 (Figure 4G). Similar synaptic punctate pattern was also evident in 2D cultures of dissociated organoids (Figure S3; n = 7 cultures). Finally, ultrastructure analysis by transmission electron microscopy (TEM) demonstrated the presence of typical synaptic structures showing synaptic vesicles and electron-dense synaptic contact sites (Figures 4H and 4I, asterisks and arrowheads, respectively; n = 3 organoids).

2D/3D cortical brain organoids showed mature function

We next tested the neurophysiological activity of organoids by multielectrode array (MEA). Five-month-old organoids were cultured in standard conditions until 2 months prior to recordings and then with either cortical organoid differentiation medium (CODM) or a physiological relevant neuronal medium (BrainPhys) up until the MEA recordings. Organoids were placed on the MEA 1 day before recordings (Figure 5A). Spontaneous firing activity was observed in organoids cultured in BrainPhys (Figures 5B and 5C), but not in CODM organoids. Similarly, spike raster plots showed firing patterns of organoids across all electrodes with marked network bursts in organoids cultured in BrainPhys only (Figures 5D, 5E, and S4). The mean firing

rate (MFR) of neurons cultured in BrainPhys was significantly greater than CODM-grown organoids (1.7 ± 1.3 Hz in BrainPhys and 0.03 ± 0.04 Hz in CODM; n = 5 organoids, N = 3 independent batches of differentiation, mean \pm SD, 60 electrodes; p = 0.0466; paired two-tailed t test) (Figure S4). Next, we performed pharmacological intervention using tetrodotoxin (TTX) as a synaptic blocker. Organoid network activity was abolished with TTX addition, with activity returning to normal levels after washout (Figure 5F; n = 5 organoids, N = 3 differentiation batches, mean \pm SD; p < 0.0001, paired two-tailed t test).

BrainPhys medium has been described as a more physiological environment supporting the basic function of neurons (Bardy et al., 2015). To gain insights into possible differences between BrainPhys and CODM-cultured organoids, we compared their proteome. Organoids were grown in parallel from the same batches of differentiation (Figures 5G and 5H; n = 3 organoids/batch, N = 3 differentiation batches, 9 organoids analyzed in total for each condition). Proteomic analysis detected 4,334 in common proteins for both conditions with an additional 27 and 242 unique BrainPhys and CODM proteins, respectively. The different culture conditions showed differences in protein enrichment (Figure 5G). Notably, enriched proteins that could potentially explain the improved function of BrainPhys-cultured neurons included synaptic vesicle-associated proteins synaptophysin (encoded by *SYP*) and synaptotagmin 1 (*SYT1*), glutamate receptor delta 1 subunit (*GRID1*) involved in synaptogenesis and phosphatase and tensin homolog (*PTEN*) responsible for synapse maturation (Figure 5H). Next, organoids were transduced with an AAV9.*SYN1* (*Synapsin 1*) promoter driving an mCherry reporter. Synapsin 1 tethers pools of synaptic vesicles in nerve terminals and has an activity-dependent function regulating the availability of synaptic vesicles for neurotransmitter release (Cesca et al., 2010). When cultured in BrainPhys, organoids showed increased neuronal *Synapsin*

Figure 4. Comparison of the iPSC and cortical organoid proteomes using Gene Ontology enrichment analysis

(A) Comparison of biological process terms with the largest difference in probability of enrichment for the genes encoding proteins detected in the iPSC and cortical organoid (CODM media) proteomes. The color scheme represents the value of $-\log_{10}(P)$, where P is the probability of enrichment adjusted by a false discovery rate of 5%. The size of each circle represents the ratio of enrichment. Absent circles indicate an enrichment ratio < 1.1.

(B) Top five biological process synaptic terms not already shown in (A).

(C) Top five biological process development terms not already shown in (A).

(D) Comparison of the KEGG pathway terms.

(E) Examples of proteins detected exclusively in either iPSCs or cortical organoids involved in maintenance of stem cells or synaptic functions.

(F and G) Immunohistochemistry images showing VGLUT1 puncta in MAP2 neuronal dendrites (G, high-magnification image of inset in F).

(H) SYNAPTOPHYSIN pre-synaptic and PSD95 post-synaptic markers.

(I and J) Ultrastructure electron microscopy images of cortical organoids showing synaptic clefts (arrowheads) and synaptic vesicles (asterisks).

Scale bars, 5 μ m (G) and 25 μ m (F and H). See also Figure S3.

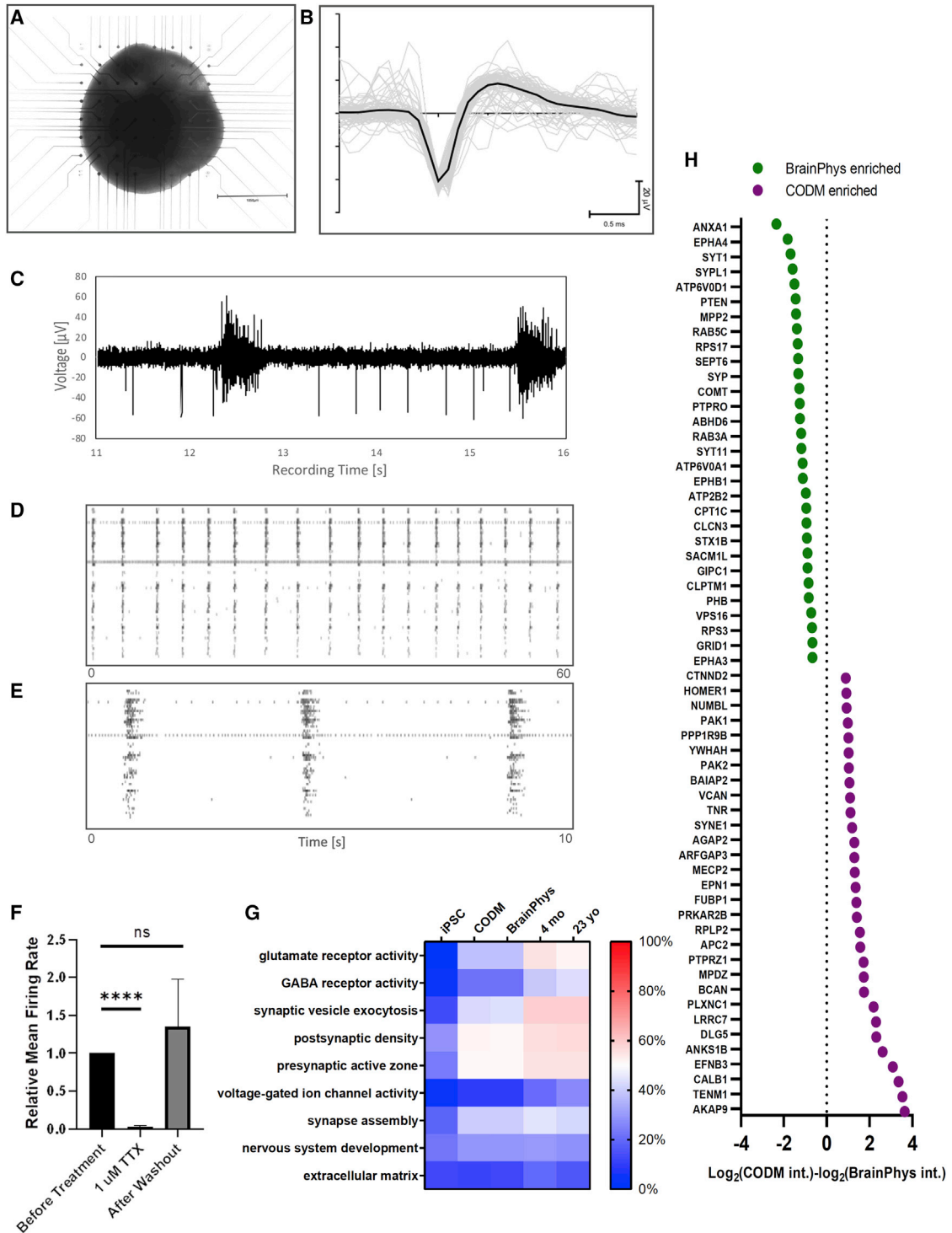


Figure 5. Cortical organoids develop synchronous networks

(A) Cortical organoid plated overnight on multi-electrode array (MEA).

(B and C) Representative spontaneous firing activity of organoid.

(D and E) Spike raster plots showing firing patterns of organoids across all electrodes with marked network bursts.

(legend continued on next page)



1 promoter activity (Figure S4; $n = 3$ organoids). We also confirmed the presence of synapses and synaptic vesicles in BrainPhys organoids using TEM (Figure S4; $n = 3$ organoids).

Co-culture of 3D retinal-cortical organoids shows retinal nerve-like bundles projecting into brain organoids

Having demonstrated the formation of cortical organoids from confluent differentiation cultures, we next aimed to test whether the 3D suspension culture of complex organoids comprising both retinal and brain organoids promoted the formation of retinal ganglion cells axonal projections between the two organs.

In early 2D differentiation cultures, retinal and brain organoids spontaneously developed in proximity, enabling the manual isolation of these two organoids for further maturation in suspension (Figure 6A). This differentiation was tested in 4 PSC lines ($n = 185$ organoids analyzed, $N > 10$ differentiation batches), including the H9.mCherry ESC line in which the typical morphology of brain neural rosettes and thick neural epithelium of retinal organoids are easily discerned. In 3D culture, at 5 weeks, the two organoids were attached but failed, at this early stage, to show any clear axonal projections (Figure 6B). The connection of the retina to the brain to process the visual information is established by RGCs, the first-born cell type of the retina, which form neuronal outputs connecting to the brain through the optic nerve. At 7 weeks, light-sheet microscopy of cleared 3D retinal-brain complex organoids ($n = 49$ organoids analyzed) enabled the visualization of MAP2-positive retinal cells present in the retina connected to brain organoids forming structures that resemble a presumptive nerve bundle (Figures 6C–6F; Figure S7; and Video S2).

At 10 weeks, the development of each individual organoid was apparent. In retinal organoids, similarly to the chick and rodent retina (Tucker and Matus, 1987; Okabe et al., 1989), MAP2 delineated RGCs which colocalized with THY1, HuC/HuD, and NeuN RGC markers delineating these cells' axonal projections toward the center of the organoid (Figure S5). CRX-positive photoreceptor cells were present in retinal organoids with RGC THY1-positive axons assembling in the middle of the retinal organoid, which then appeared to extend axonal processes to the TBR1- and THY1-positive brain organoid (Figures 6G and 6H; $n = 13$ organoids, $N = 9$ differentiation batches; Figure S6). Finally, to specifically identify RGCs and their axonal pro-

jections, retinal organoids were generated from an ESC H7.BRN3b-P2A-mCherry reporter line (Sluch et al., 2015). At 8.5 weeks, mCherry-positive cells showed co-expression with numerous RGC markers, and their axons were readily identified in retinal organoids forming a nerve fiber-like layer (Figure 7; Figure S6). Consecutive sections through complex organoids demonstrated the morphological differences of the two organoids (Figures 7A–7H and 7I–7L; non-fused organoids) with nerve-like structures crossing into the brain organoid (Figures 7A, 7I, and 7K, arrows). Nerve-like bundles were also observed crossing the middle of retinal organoids (Figures 7B–7D; Figure 7H, high magnification of boxed area in Figure 7D). All BRN3b.mCherry organoids contained axonal projections within brain organoids (Figure 7, arrowheads; $n = 19$ organoids, $N = 3$ differentiation batches). In $27\% \pm 11\%$ of non-fused organoids the RGC axonal outgrowths reached the end of the brain organoid, and in $24\% \pm 8\%$ mCherry axonal projections only reached short distances close to the nerve entry point. Interestingly, $48\% \pm 10\%$ of retinal-brain organoids naturally fused in culture (Figure 7Q; fused organoids; mean \pm SD), and of these, all organoids showed long and abundant axonal projections extending throughout the organoid (Figures 7M–7P). These mCherry retinal axonal projections were observed in proximity to neuronal (SOX2 and CTIP2) and nascent-glial populations (S100B) in the brain organoids (Figures S7C and S7D). Light-sheet microscopy of BRN3b.mCherry also demonstrated RGC axons in the retinal organoid-forming nerve-like structures that crossed from the center of the retina toward the brain organoid ($n = 3$ organoids imaged; Figures S7E–S7I; Video S3). Brain regions were positive for the synaptic vesicle membrane protein Synaptophysin (SYP). Importantly, these synaptic vesicles were also observed in brain regions populated by RGC mCherry axons (Figures 7R and 7S).

Finally, we performed gene expression analysis in retinal, retinal-brain, and brain organoids from the same differentiation batch (Figures S7J–S7L, bright-field images) for *PCP4* and *LHX9*, which are both expressed in the lateral geniculate nucleus (LGN), the RGC target, and the relay station for visual input in the brain (Iwai and Kawasaki, 2009). We also analyzed *ZIC2*, a transcription factor involved in RGC axon guidance and highly expressed in the optic tract (Herrera and Mason, 2003). A significant increase in gene expression fold change for *PCP4* and *ZIC2* was observed for retinal-brain organoids compared with brain and retinal organoid samples (Figure 7V; $n = 6$ organoids per sample, $N = 3$ independent differentiation batches;

(F) TTX treatment abolished firing activity, which returned following washing (mean \pm SD, paired two-tailed t test, **** $p < 0.0001$).

(G) Heatmap showing proteome comparison of iPSC, organoids, 4 months, and 23-year-old brain.

(H) Proteins differentially enriched in organoids cultured in CODM or BrainPhys media ($p < 0.05$, adjusted by a false discovery rate of 5%). See also Figure S4.

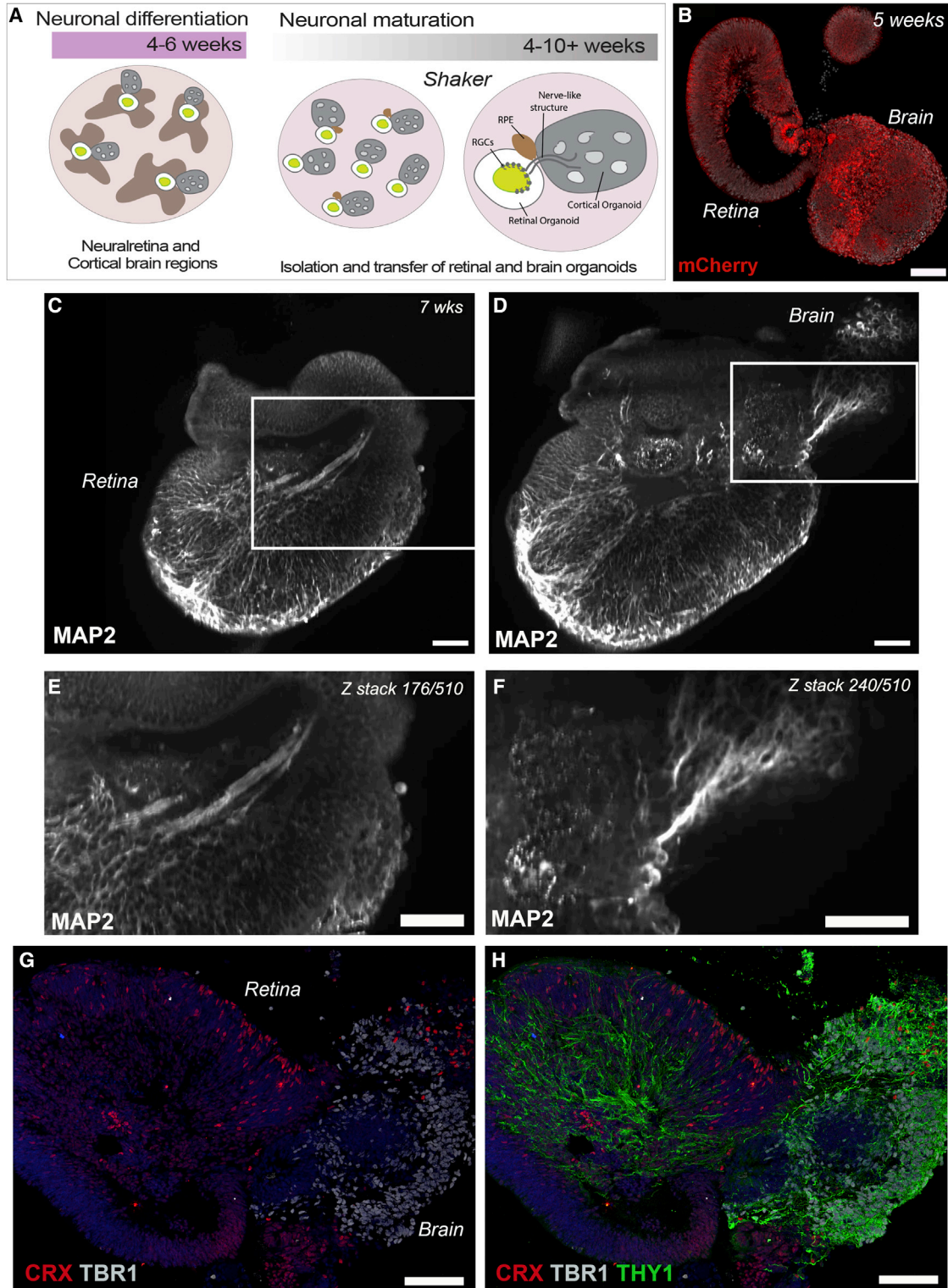


Figure 6. Complex retinal-cortical organoids form optic nerve-like structures

(A) Schematic illustrating the timeline of neuronal differentiation.

(B) Week 5 H9 ESC.mCherry retinal-brain organoid showing typical morphologies of retinal and brain regions growing together.

(legend continued on next page)



two-way ANOVA and Fisher's least significant difference [LSD] test, $p < 0.05$ [significance of average $\Delta\Delta Ct_{\pm}$ value]).

DISCUSSION

PSC-derived retinal and brain organoids have utility for disease modeling, particularly neurodegeneration of both eye and brain. Although numerous differentiation protocols have been described, these differ considerably in methodology: some rely entirely on the addition of growth factors and matrices to guide cell fate decisions and organ formation, while others form spontaneous organoids through the endogenous potential of PSCs to form the niches *in vitro*. Variability among protocols and in-batch organoid variability is a common problem of both approaches. Other challenges include the phenotypical and maturity differences between *in vitro*-generated cells and their *in vivo* counterparts. Furthermore, the generation of the right cell type to enable the analysis of functional assays and testing of new therapies requires long-term cultures. Each of these protocols presents its own advantages and disadvantages, and thus the initial choice of protocol is important.

Here, we adapted a previously described simple and robust 2D/3D differentiation approach derived from confluent cultures of PSCs (Reichman et al., 2014) and generated cortical organoids within the same cultures of retinal vesicles and RPE cells. Brain organoids form the neural rosettes, a feature that enabled their ready isolation. This differentiation method only requires a confluent culture of PSCs followed by change to a pro-neural induction media and does not require the addition of Matrigel or exogenous factors. We confirmed the generation of dorsal cortical organoids that express typical cortical plate neurons as well as inhibitory and excitatory neurons and glial populations.

Omics analysis of PSC lines and their initial stage of differentiation have shed light on the variability between cell lines leading to increased differences between organoids generated among multiple cell lines (Quadrato et al., 2017). Our undirected protocol enabled reproducibility of directed organoids but with the benefits of spontaneous differentiations.

Despite tremendous progress in the field, the lack of disease-relevant functional assays in organoids hinders their

ability to test for new treatment efficacy. However, disease molecular signatures and biomarkers can be determined using integrative analysis of omics as well as computational or bioinformatic methodologies. In this study, our cortical organoids were extensively characterized using scRNA-seq and proteomics analysis. In agreement with a previous correlation study comparing scRNA-seq datasets of brain organoids (Tanaka et al., 2020), our organoids showed a high correlation with dorsally patterned brain organoids generated in the directed differentiation approach demonstrated in Velasco et al. (2019), known for their reproducibility.

The proteome of brain organoids has been seldom investigated. Previous proteomic analysis of early staged (day 45) brain organoids generated using a whole-brain spontaneous 3D method highlighted the protein-protein interactions involved in early neuronal specification (Nascimento et al., 2019). Our proteomic analysis demonstrated expression of proteins related to neuronal development and synaptic function in the cortical organoids and a relative decrease in cell cycle-related proteins. The detection of synaptic protein components was further corroborated by IHC for synaptic markers and ultrastructure electron microscopy.

Neuronal network formation in brain organoids have previously been studied elegantly in late-stage organoids cultured on the MEA for a few months (Quadrato et al., 2017; Trujillo et al., 2019). Our electrophysiology analysis verified the functionality of cortical organoids, demonstrating their synchronous neuronal network activity when cultured in an electrophysiologically relevant medium, BrainPhys (Bardy et al., 2015). A separate proteomics analysis identified proteins enriched in the BrainPhys-cultured organoids that might explain how BrainPhys media promotes favorable electrophysiological activity. Overall, these results demonstrate the generation of functional cortical organoids.

Neurodevelopmental disorders leading to higher order cognitive abilities mostly affect the cortex, and thus modeling of these conditions using cortical organoids is crucial (Zhao and Bhattacharyya, 2018). In the eye, modeling of more complex disease traits requires the differentiation of specific brain regions and their functional integration as well as their connection with other organs. The formation of retinal vesicles and optic cups from brain

(C–F) Light-sheet image of whole retinal-brain organoid showing consecutive z stack images of MAP2 retinal ganglion cells axons. (E and F) High-magnification images from insets in (C) and (D) show axonal nerve-like structure projecting toward the central part of retinal organoid (E, z stack 176 out of 510 stacks). Deeper z stack 240 showing the same axonal projection connecting to brain region (F). (G) CRX-positive photoreceptors in retinal organoids and TBR1 neurons in brain organoids. (H) THY1-positive retinal ganglion cells send axonal projections to the center of the retinal organoid that connect with brain organoid TBR1/THY1-positive neurons in brain regions. Scale bars, 100 μ m (B, G, H) and 200 μ m (C–F). Cell lines used for (C)–(H) include HPSI0314i-hoik_1, H9 WiCell ES, and TiPSC-5 iPS. See also Figure S6.

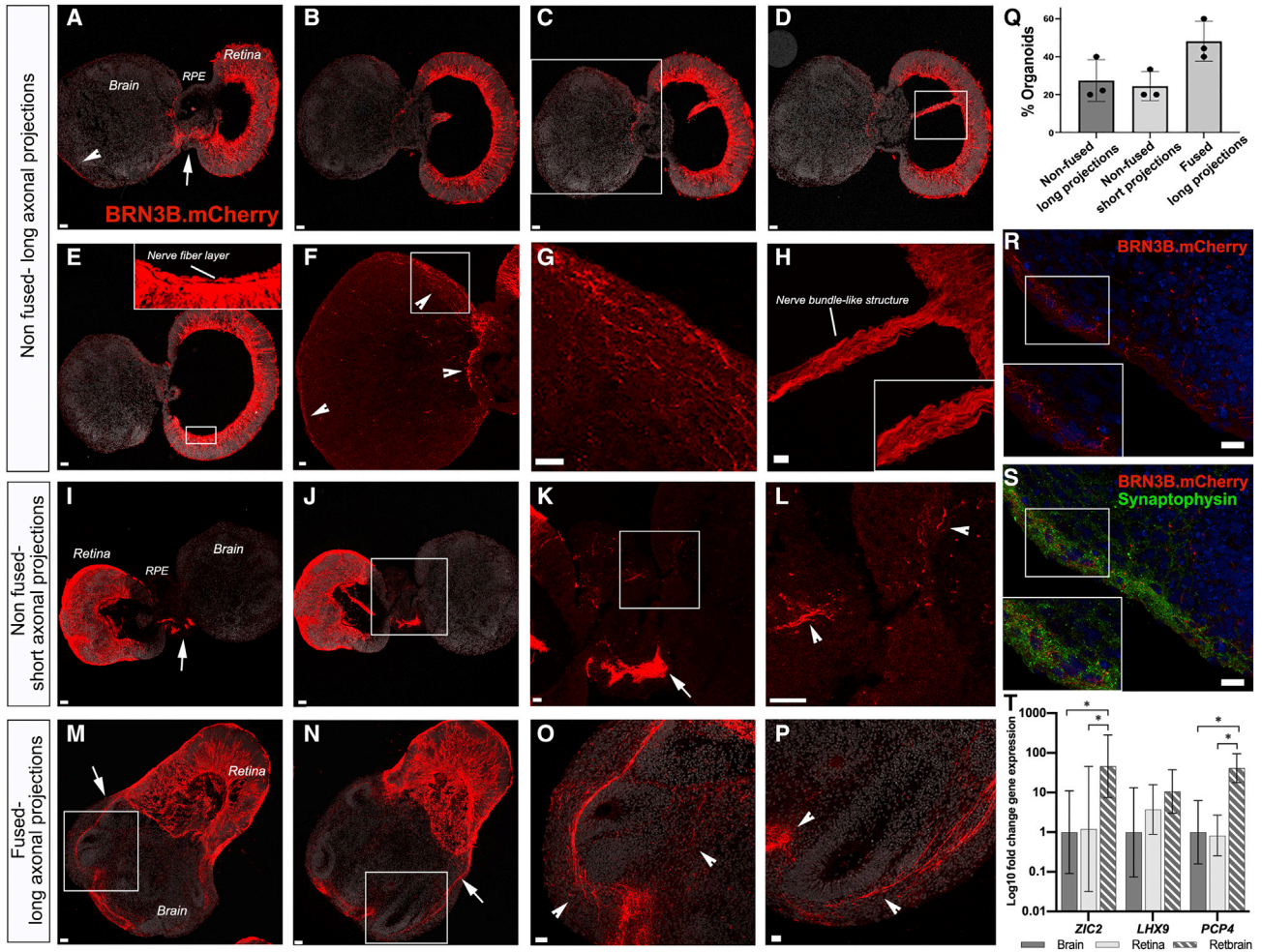


Figure 7. RGCs axonal projections into brain organoids

(A–P) Images of consecutive sections through a week 8.5 retinal-brain complex organoids generated from BRN3b.mCherry ESC line. (A–L) Retinal and brain organoids are clearly visible and separated by RPE (non-fused). Retinal organoids show numerous mCherry-positive RGCs, which extend axonal projections (arrow) into the brain organoid. Axonal outgrowths coming from RGCs are observed in the far end of the brain organoid (arrowheads). (B–D) Nerve-like bundle structures are also observed crossing the retinal organoid towards the brain. (F and G) High magnification of inset in (C) is shown in (F) and (G) showing axonal projections in the brain organoid. (H) High-magnification image of inset (D) shows a nerve-fiber layer forming in the retinal organoid (also shown in E) and the formation of nerve bundle-like structures crossing the retinal organoid (H). (I–L) Another example of non-fused retinal and brain organoid showing a nerve-like structure crossing the middle of the retinal organoid and connecting into the brain organoid (arrows in I and K, high-magnification image from inset in J). Short axonal projections are observed only in the initial crossing point into the brain organoid (L, arrowheads; high-magnification image from inset in K). (M–P) Example of retinal and brain organoids that fused while in suspension culture. Brain organoids show extensive axonal outgrowths covering the whole brain organoid (M and N, arrows; O and P, high-magnification panels from insets in M and N, arrowheads). (Q) Percentage of fused and non-fused organoids and their axonal outgrowths phenotypes (mean \pm SD). (R and S) Synaptophysin is observed in brain regions populated by mCherry retinal axons. (T) Fold change in gene expression in retinal and retinal-brain organoids in comparison with brain organoids (error bars show SD reported as log fold change; two-way ANOVA and Fisher's LSD test, $*p < 0.05$). Scale bars, 20 μ m (G–L, O, P, R, and S), 40 μ m (A–F, I, J, M, and N). See also Figure S7.

regions in 3D organoid cultures has been demonstrated in seminal studies (Kuwahara et al., 2015; Nakano et al., 2012), including a recent study showing bilateral optic vesicles (Gabriel et al., 2021).

Here, we demonstrated the spontaneous formation of retinal and brain complex organoids in 2D/3D confluent cultures. When in 3D suspension, these retinal-brain organoids connect through a nerve-like structure mimicking



the neuronal projections that connect the eye and brain. Our confluent method of differentiation enabled the precise isolation of these two organoids, overcoming variability within 3D directed and whole-brain protocols that sporadically generate eye structures (Lancaster et al., 2013; Quadrato et al., 2017) and the forced fusion of different organoids to form assembloids. The latter have been successfully used to model *in vivo* neuronal interactions between different brain regions (Bagley et al., 2017; Birey et al., 2017; Miura et al., 2020; Xiang et al., 2019) and most recently retinofugal projections between eye and brain regions (Fligor et al., 2021). Here we offer an alternative method to assembloid formation.

We used numerous cell lines and axonal markers to demonstrate the emerging RGC axonal projections between retinal and brain organoids. The mature myelinated optic nerve includes close contact with brain astrocyte cells, which have migrated into the retina during development and vasculature formation. Here, at the early stages analyzed, we simply demonstrate the formation of nerve bundles that cross into brain organoids extending axonal projections. We have demonstrated the presence of S100B glial populations in brain organoids in proximity to BRN3b.mCherry RGC axons; however, as expected for the early time points analyzed, these cells were not observed close to retinal organoids, suggesting that migration of astrocytes from brain to RGC layer has not taken place. Furthermore, no clear myelination was observed in the retinal nerve-like bundles. The formation of mature optic nerve-like structures will elucidate the dynamics of retinogenesis and neurogenesis that can then be used to model a number of optic neuropathies, such as glaucoma. Retinal-brain organoids also promise to improve organoid development, such as the long-term survival and maturation of RGCs, as these cells no longer lack their contact with the output in the cortex (Fligor et al., 2021). Neurodegeneration in glaucoma is complex and extends beyond the eye into the LGN and visual cortex (Gupta et al., 2006) of the brain. Similarly, late-onset neurodegenerative diseases, such as Alzheimer's disease, show early phenotypes in the eye (Ning et al., 2008), which enables pre-symptomatic diagnosis (Hadoux et al., 2019). Accurate models of such diseases will elucidate novel aspects of disease pathogenesis and aid the challenges of developing effective treatments.

Our data demonstrate the undirected derivation of both cortical and retinal organoids from a confluent culture of PSCs. The simplicity of this differentiation method coupled with the ease of precisely locating cortical organoids addresses the current problems of in-batch organoid-to-organoid variability. The comprehensive characterization shown here, including novel proteome data of brain organoids, expands the available repertoire of relevant models of human disease. Importantly,

this method also enabled the formation of complex organoid-forming nerve-like structures that resemble the important connection between the retina and the brain, the optic nerve. Future investigations including further culture development of these retinal-brain complex organoids will possibly enable the formation of a mature optic nerve and allow the study of common optic nerve neuropathies.

EXPERIMENTAL PROCEDURES

Derivation of UCLOO017-A-1 and UCLIO009-A-3 induced pluripotent stem cell lines

Peripheral blood mononuclear cells were isolated from the whole blood of a healthy donor using density gradient centrifugation. Briefly, 25 mL whole blood diluted 1:1 with PBS was layered on top of 15 mL of Ficoll-Paque Premium and centrifuged with brake and accelerator off at $500 \times g$ for 30 min, and the cloudy interphase containing peripheral blood mononuclear cells (PBMCs) was collected. Two million cells were cultured for 6 days in hematopoietic expansion media StemSpan H3000, with the addition of EPO, IL-3, dexamethasone, ascorbic acid, SCF, and IGF-1. Following expansion, 200,000 cells were nucleofected using Amaxa 4D nucleofector with Addgene plasmids. The nucleofected cells were plated on a well of a 6-well plate coated with Geltrex matrix and transitioned to Essential 8 media. Obtained iPSC clones were further cultured for 10 passages prior to characterization.

Differentiation of PSC into cortical organoids

Human iPSCs were maintained until 90% confluent as described above. Media was replaced with Essential 6 (E6) media for 2 consecutive days. At day 3 of differentiation, E6 media was replaced with a pro-neural induction media (PIM; composed of advanced DMEM/F12, 1% N_2 supplement, 1% L-glutamine, 1% non-essential amino acids, and 1% antibiotic-antimycotic). At around weeks 3–4 of culture, 3D organoids containing rosettes were observed throughout the plate and in close proximity to neuroretinal vesicles. Cortical organoids were manually excised and maintained in 60-mm-well plates in retinal differentiation media (RDM; composed of DMEM, 30% F12 nutrient mix, 2% B27-vitamin A, and 1% antibiotic-antimycotic) on an orbital shaker at 85 rpm. At 6 weeks of differentiation, retinal differentiation medium was supplemented with 10% fetal bovine serum (FBS), 100 μ M taurine, and 2mM GlutaMAX. At 10 weeks, cortical organoids were cultured in a cerebral organoid differentiation medium as described in Lancaster et al. (2013) (50% neurobasal medium, 50% DMEM/F12, 0.5% N_2 supplement, 0.03% insulin, 1% GlutaMAX, MEM-NEAA, B-mercaptoethanol, 1% B27 supplement) or BrainPhys hPSC Neuron Kit (Stem Cell Technologies, BrainPhys Neuronal medium, NeuroCult SM1 neuronal supplement, 1% N_2 supplement, human recombinant BDNF and GDNF, ascorbic acid and dibutyryl-cAMP). iPSC line UCLOO017-A-1 was used in most of the main figures. In Figure 6, cell lines used included ESC WiCell H9.mCherry (Figure 6B), HPSI0314i-hoik_1 (Figures 6C–6F), and TiPSC-5 (Figures 6G and 6H). In Figure 7, ESC H7 WA07 A81.BRN3B-P2A-mCherry was used.



Immunohistochemistry

Brain organoids were washed with PBS and fixed for 40–60 min in 4% paraformaldehyde prior to incubation in 20% sucrose. Organoids were embedded in OCT and frozen in liquid nitrogen. Brain organoids were cryo-sectioned at 14 μm thickness. Cryosections were blocked in 5% serum in blocking solution (1% BSA in PBS with 0.1% Triton X) for 2 h. Primary antibody (Table S3) diluted in blocking solution was incubated overnight at 4°C. Sections were washed with PBS and incubated with secondary antibody (Alexa Fluor 488, 546, and 633 secondary antibodies) at room temperature for 2 h. Sections were counter-stained with DAPI. For IHC numbers, see Table S4.

Single-cell RNA sequencing

Organoids were dissociated as described above, and a subset of cell suspension was stained with 0.4% trypan blue and assessed for viability and concentration using Countess II Automated Cell Counter. Single-cell suspensions were passed through a 40 μm cell strainer, and concentration was adjusted to 1,000 cells/ μL . The suspension was loaded in single-cell B Chip for target output of 10,000 cells per sample. Single-cell droplet capture was performed on the Chromium Controller (10X Genomics). cDNA library preparation was performed in accordance with the Single-Cell 3' version 3 protocol. Libraries were evaluated for fragment size and concentration using Agilent HSD5000 ScreenTape System. Samples were sequenced on an Illumina NovaSeq 6000 instrument according to the manufacturer's instructions. Sequencing was carried out using a 2 \times 150 paired-end (PE) configuration with a sequencing depth of 40,000 reads per cell. The sequences were processed by GENEWIZ.

Recording of organoid activity on MEA

Organoid electrical activity was measured using an MEA2100-lite system with TC01 temperature control (Multi Channel Systems), heated to 37°C. Recordings were made for 5–10 min at a frequency of 10 kHz using Multi Channel Experimenter software. Data were processed using Multi Channel Analyzer software. Raw electrode recordings were filtered sequentially with a 200 Hz second-order Butterworth high-pass filter, then a 3 kHz second-order Butterworth low-pass filter. Spikes were picked using a threshold of 5 SDs below mean voltage for each electrode.

Organoids preparation for mass spectrometry

Organoids were isolated and cultured for 10 weeks. Three of these organoids were cultured in either CODM or BrainPhys medium for two weeks. Organoids were homogenized and lysed with a drill and pestle in 200 μL 2% SDS lysis buffer (2% [w/v] SDS, 50 mM HEPES [pH 7.4], 2 mM EGTA, 2 mM EDTA, 2 mM phenylmethylsulfonyl fluoride [PMSF], EDTA-free Protease Inhibitor [Roche], and PhosSTOP [Roche]) and freezing on dry ice. Frozen lysate was thawed and reduced with 10 mM tris(2-carboxyethyl)phosphine (TCEP) at 85°C for 10 min with shaking. Samples were alkylated with 20 mM iodoacetamide for 30 min at 23°C in the dark. Protein was precipitated using the chloroform-methanol method and pellet reconstituted in 20 μL of 7.8M urea and 50 mM HEPES (pH 8.0). Protein was digested with 3 μg Lys-C (FUJIFILM Wako Pure Chemical Corporation) and incubated for 8 h at 25°C, with shaking.

Samples were diluted 8-fold with 50 mM HEPES (pH 8.0) and digested by the addition of 5 μg TrypZean recombinant trypsin and incubation for 8 h at 30°C, with shaking. About 50 μg aliquots of each sample were desalted. Samples were eluted in 50% acetonitrile, dried, and then reconstituted in 90% acetonitrile and 0.1% trifluoroacetic acid (TFA) for hydrophilic interaction chromatography (HILIC) fractionation.

Statistical analysis

All means are presented as mean \pm SD; N denotes number of independent experiments (i.e., differentiation batches, proteome samples, or MEA measurements; n denotes number of images or retinal organoids examined, where appropriate. Statistical differences between two groups were tested using two-tailed paired and unpaired t tests. The test used is specified in figure legends and main text. Statistical significance was assessed using GraphPad Prism software.

Data and code availability

The scRNA sequencing data have been deposited in NCBI's Gene Expression Omnibus and are accessible using GEO Series accession number GSE174232 (<https://www.ncbi.nlm.nih.gov/geo/query/acc.cgi?acc=GSE174232>).

The proteomics data have been deposited to the ProteomeXchange Consortium via the PRIDE partner repository with dataset identifier PXD025933 and <http://dx.doi.org/10.6019/PXD025933>.

SUPPLEMENTAL INFORMATION

Supplemental information can be found online at <https://doi.org/10.1016/j.stemcr.2022.04.003>.

AUTHOR CONTRIBUTIONS

Conceptualization, M.F., S.L., and A.G.-C.; Methodology, J.R.W., G.C.S., B.Y.L., M.O.-W., D.X., and H.J.K.; Investigation, M.F., S.L., J.R.W., G.C.S., B.L., M.O.-W., D.X., and H.J.K.; Resources, R.R.A., T.W., and E.T.T.; Writing – Original Draft, M.F., S.L., A.G.-C.; Writing – Review & Editing, R.R.A., P.Y., M.E.G., and A.G.C.; Supervision, P.Y., M.E.G., and A.G.C.; Funding Acquisition, A.G.C.

CONFLICTS OF INTEREST

The authors declare no competing interests.

ACKNOWLEDGMENTS

We thank the Children's Medical Research Institute, Advanced Microscopy Centre, the Single Cell Analytics Facility, and the Biomedical Proteomics Facility. Electron microscopy was performed at the Westmead Scientific Platforms. Cell line iPSC TiPSC-5 was kindly provided by Prof. Yvan Arsenijevic and Prof. David Gamm and the WiCell H7 A81.BRN3B-P2A-mCherry ESC line by Prof. Donald Zack and Prof. Alice Pebay. This work is supported by Luminesce Alliance (PPM1 K5116/RD274). Luminesce Alliance was established with the support of the Government of New South Wales to coordinate and integrate pediatric research in New South Wales. The graphical abstract was generated using BioRender (<https://biorender.com>).



Received: August 6, 2021

Revised: April 4, 2022

Accepted: April 5, 2022

Published: May 5, 2022

REFERENCES

- Bagley, J.A., Reumann, D., Bian, S., Lévi-Strauss, J., and Knoblich, J.A. (2017). Fused cerebral organoids model interactions between brain regions. *Nat. Methods* *14*, 743–751.
- Bardy, C., Van den Hurk, M., Eames, T., Marchand, C., Hernandez, R.V., Kellogg, M., Gorris, M., Galet, B., Palomares, V., Brown, J., et al. (2015). Neuronal medium that supports basic synaptic functions and activity of human neurons in vitro. *Proc. Natl. Acad. Sci.* *112*, E2725–E2734.
- Birey, F., Andersen, J., Makinson, C.D., Islam, S., Wei, W., Huber, N., Fan, H.C., Metzler, K.R.C., Panagiotakos, G., Thom, N., et al. (2017). Assembly of functionally integrated human forebrain spheroids. *Nature* *545*, 54–59.
- Cesca, F., Baldelli, P., Valtorta, F., and Benfenati, F. (2010). The synapsins: key actors of synapse function and plasticity. *Prog. Neurobiol.* *91*, 313–348.
- Cordero, A.G., Kruczek, K., Naeem, A., Fernando, M., Kloc, M., Ribeiro, J., Goh, D., Duran, Y., Blackford, S.J.L., Abelleira-Hervas, L., et al. (2017). Recapitulation of human retinal development from human pluripotent stem cells generates transplantable populations of cone photoreceptors. *Stem Cell Rep.* *9*, 820–837.
- Fligor, C.M., Lavekar, S.S., Harkin, J., Shields, P.K., VanderWall, K.B., Huang, K.-C., Gomes, C., and Meyer, J.S. (2021). Extension of retinofugal projections in an assembled model of human pluripotent stem cell-derived organoids. *Stem Cell Rep.* *16*, 2228–2241.
- Gabriel, E., Albanna, W., Pasquini, G., Ramani, A., Josipovic, N., Mariappan, A., Schinzel, F., Karch, C.M., Bao, G., Gottardo, M., et al. (2021). Human brain organoids assemble functionally integrated bilateral optic vesicles. *Cell Stem Cell* *28*, 1740–1757.e8.
- Gupta, N., Ang, L.-C., deTilly, L.N., Bidaisee, L., and Yücel, Y.H. (2006). Human glaucoma and neural degeneration in intracranial optic nerve, lateral geniculate nucleus, and visual cortex. *Br. J. Ophthalmol.* *90*, 674.
- Hadoux, X., Hui, F., Lim, J.K.H., Masters, C.L., Pébay, A., Chevalier, S., Ha, J., Loi, S., Fowler, C.J., Rowe, C., et al. (2019). Non-invasive in vivo hyperspectral imaging of the retina for potential biomarker use in Alzheimer's disease. *Nat. Commun.* *10*, 4227.
- Herrera, E., and Mason, C. (2003). Zic2 patterns binocular vision by specifying the uncrossed retinal projection. *Cell* *115*, 125.
- Iwai, L., and Kawasaki, H. (2009). Molecular development of the lateral geniculate nucleus in the absence of retinal waves during the time of retinal axon eye-specific segregation. *Neuroscience* *159*, 1326–1337.
- Kuwahara, A., Ozone, C., Nakano, T., Saito, K., Eiraku, M., and Sasai, Y. (2015). Generation of a ciliary margin-like stem cell niche from self-organizing human retinal tissue. *Nat. Commun.* *6*, 6286.
- Lancaster, M.A., Renner, M., Martin, C.-A., Wenzel, D., Bicknell, L.S., Hurler, M.E., Homfray, T., Penninger, J.M., Jackson, A.P., and Knoblich, J.A. (2013). Cerebral organoids model human brain development and microcephaly. *Nature* *501*, 373–379.
- Lin, Y., Cao, Y., Kim, H.J., Salim, A., Speed, T.P., Lin, D.M., Yang, P., and Yang, J.Y.H. (2020). scClassify: sample size estimation and multiscale classification of cells using single and multiple reference. *Mol. Syst. Biol.* *16*, e9389.
- Miura, Y., Li, M.-Y., Birey, F., Ikeda, K., Revah, O., Thete, M.V., Park, J.-Y., Puno, A., Lee, S.H., Porteus, M.H., et al. (2020). Generation of human striatal organoids and cortico-striatal assembloids from human pluripotent stem cells. *Nat. Biotechnol.* *38*, 1421–1430.
- Nakano, T., Ando, S., Takata, N., Kawada, M., Muguruma, K., Sekiguchi, K., Saito, K., Yonemura, S., Eiraku, M., and Sasai, Y. (2012). Self-formation of optic cups and storable stratified neural retina from human ESCs. *Cell Stem Cell* *10*, 771–785.
- Nascimento, J.M., Saia-Cereda, V.M., Sartore, R.C., da Costa, R.M., Schitine, C.S., Freitas, H.R., Murgu, M., Reis, R.A. de M., Rehen, S.K., and Martins-de-Souza, D. (2019). Human cerebral organoids and fetal brain tissue share proteomic similarities. *Front. Cell Dev. Biol.* *7*, 303.
- Ning, A., Cui, J., To, E., Ashe, K.H., and Matsubara, J. (2008). Amyloid- β deposits lead to retinal degeneration in a mouse model of Alzheimer disease. *Invest. Ophthalm. Vis. Sci.* *49*, 5136–5143.
- Okabe, S., Shiomura, Y., and Hirokawa, N. (1989). Immunocytochemical localization of microtubule-associated proteins 1A and 2 in the rat retina. *Brain Res.* *483*, 335–346.
- Paşca, A.M., Sloan, S.A., Clarke, L.E., Tian, Y., Makinson, C.D., Huber, N., Kim, C.H., Park, J.-Y., O'Rourke, N.A., Nguyen, K.D., et al. (2015). Functional cortical neurons and astrocytes from human pluripotent stem cells in 3D culture. *Nat. Methods* *12*, 671–678.
- Qian, X., Song, H., and Ming, G. (2019). Brain organoids: advances, applications and challenges. *Development* *146*, dev166074.
- Quadrato, G., Nguyen, T., Macosko, E.Z., Sherwood, J.L., Yang, S.M., Berger, D.R., Maria, N., Scholvin, J., Goldman, M., Kinney, J.P., et al. (2017). Cell diversity and network dynamics in photosensitive human brain organoids. *Nature* *545*, 48–53.
- Reichman, S., Terray, A., Slembrouck, A., Nanteau, C., Orioux, G., Habeler, W., Nandrot, E.F., Sahel, J.A., Monville, C., and Goureau, O. (2014). From confluent human iPS cells to self-forming neural retina and retinal pigmented epithelium. *Proc. Natl. Acad. Sci. U S A* *111*, 8518–8523.
- Reichman, S., Slembrouck, A., Gagliardi, G., Chaffiol, A., Terray, A., Nanteau, C., Potey, A., Belle, M., Rabesandratana, O., Duebel, J., et al. (2017). Generation of storable retinal organoids and retinal pigmented epithelium from adherent human iPS cells in Xeno-free and Feeder-free conditions. *Stem Cells* *35*, 1176–1188.
- Sinn, R., and Wittbrodt, J. (2013). An eye on eye development. *Mech. Dev.* *130*, 347–358.
- Sluch, V.M., Davis, C.O., Ranganathan, V., Kerr, J.M., Krick, K., Martin, R., Berlinicke, C.A., Marsh-Armstrong, N., Diamond, J.S., Mao, H.-Q., et al. (2015). Differentiation of human ESCs to retinal ganglion cells using a CRISPR engineered reporter cell line. *Sci. Rep.* *5*, 16595.



- Tanaka, Y., Cakir, B., Xiang, Y., Sullivan, G.J., and Park, I.-H. (2020). Synthetic analyses of single-cell transcriptomes from multiple brain organoids and fetal brain. *Cell Rep.* *30*, 1682–1689.e3.
- Trujillo, C.A., Gao, R., Negraes, P.D., Gu, J., Buchanan, J., Preissl, S., Wang, A., Wu, W., Haddad, G.G., Chaim, I.A., et al. (2019). Complex oscillatory waves emerging from cortical organoids model early human brain network development. *Cell Stem Cell* *25*, 558–569.e7.
- Tucker, R.P., and Matus, A.I. (1987). Developmental regulation of two microtubule-associated proteins (MAP2 and MAP5) in the embryonic avian retina. *Development* *101*, 535–546.
- Velasco, S., Kedaigle, A.J., Simmons, S.K., Nash, A., Rocha, M., Quadrato, G., Paulsen, B., Nguyen, L., Adiconis, X., Regev, A., et al. (2019). Individual brain organoids reproducibly form cell diversity of the human cerebral cortex. *Nature* *570*, 523–527.
- Xiang, Y., Tanaka, Y., Cakir, B., Patterson, B., Kim, K.-Y., Sun, P., Kang, Y.-J., Zhong, M., Liu, X., Patra, P., et al. (2019). hESC-derived thalamic organoids form reciprocal projections when fused with cortical organoids. *Cell Stem Cell* *24*, 487–497.e7.
- Zhao, X., and Bhattacharyya, A. (2018). Human models are needed for studying human neurodevelopmental disorders. *Am. J. Hum. Genet.* *103*, 829–857.